RSC Advances

PAPER

View Article Online
View Journal | View Issue



Cite this: *RSC Adv.*, 2017, **7**, 3072

# Formation of uniform PbS quantum dots by a spin-assisted successive precipitation and anion exchange reaction process using $PbX_2$ (X = Br, I) and $Na_2S$ precursors†

Jin Hyuck Heo,‡[ab] Min Hyeok Jang,‡[a] Min Ho Lee,[a] Myoung Sang You,[a] Sang-Wook Kim,[b] Jae-Joon Lee[c] and Sang Hyuk Im*[a]

Received 21st October 2016
Accepted 22nd November 2016

DOI: 10.1039/c6ra25637f

www.rsc.org/advances

We devised a straightforward spin-assisted successive precipitation and anion exchange reaction (spin-SPAER) process in order to deposit relatively uniform PbS quantum dots (QDs) on mesoporous $TiO_2$ (mp-$TiO_2$). For the spin-SPAER process, we used $PbX_2$ (X = I, Br, and Cl) precursors instead of a $Pb(NO_3)_2$ precursor and consequently deposited individual PbS QDs on mp-$TiO_2$ due to the suppressed overgrowth of PbS QDs, whereas the conventional spin-assisted successive ionic layer adsorption and reaction (spin-SILAR) process formed aggregated PbS QDs on the mp-$TiO_2$ surface due to continuous adsorption and reaction. In addition, the PbS QDs prepared by spin-SPAER showed better air stability than the PbS QDs prepared by spin-SILAR possibly due to the passivation by halogen elements such as I and Br. Accordingly, we could improve the overall power conversion efficiency of PbS QD-SSCs prepared by the spin-SPAER process using $PbI_2$ and $PbBr_2$ precursors to ~26.7% and ~44.2%, respectively, compared to the PbS QD-SSCs prepared by spin-SILAR using the $Pb(NO_3)_2$ precursor.



Metal chalcogenide, such as CdSe,[1] CdTe,[2] PbS,[3] PbSe,[4] $Sb_2S_3$,[5] $Sb_2Se_3$,[6] $Sb_2S_{3-x}Se_x$,[7] HgTe,[8] $CISe_2$,[9] and $CITe_{2-x}Se_x$,[10] semiconductor- or quantum dot (QD)-sensitizers have been considered as promising candidates replacing the conventional Ru/organic dye sensitizer because of their unique properties such as high absorptivity, convenient bandgap tailoring, easy charge separation by a large dipole moment, and solution processability.[11]

Among the metal chalcogenides, PbS QDs have been extensively studied because they are an ideal model light absorber due to their large Bohr radius, small bulk bandgap energy, strong absorptivity, wide absorption spectrum from visible to near infrared, and multiple exciton generation. PbS QD solar cells can be roughly classified as Schottky,[12] depleted heterojunction,[13] or sensitized type,[14] with respect to the device architecture. Unlike Schottky and depleted heterojunction type devices, the sensitized solar cells have unique device architecture of electron conductor, sensitizer, and hole conductor, which can promptly transfer charge carriers into electron conductor and hole conductor. Occasionally the depleted heterojunction PbS QD solar cells exhibited higher device efficiency than the PbS QD-sensitized solar cells (QD-SSCs), the sensitized solar cells still have advantages to attain high efficiency with low cost in terms of device architecture and operating mechanism so that continuous studies are needed.

The PbS QD-SSCs are generally fabricated by depositing the PbS colloidal QDs (CQDs) on a mesoporous $TiO_2$ (mp-$TiO_2$) electron conductor or directly growing the PbS QDs on the mp-$TiO_2$ *via* successive ionic layer adsorption and reaction (SILAR) method. The PbS CQDs have uniform size distribution so that they are good for injecting the electrons from PbS CQDs into mp-$TiO_2$ because their conduction band edge can be uniformly positioned over the conduction band edge of mp-$TiO_2$. However, their surfaces are passivated by insulating long alkyl chains in order to make uniform sized PbS CQDs *via* hot-injection method. Therefore, the insulating long alkyl ligands are replaced to short ligands such as 1,2-ethane dithiol (EDT), 3-mercaptopropionic acid (MPA), and halogens to improve the charge transport at mp-$TiO_2$/PbS CQDs interface and PbS CQDs bulk. For instance, Im *et al.* reported 2.9% multiple-layered PbS QD-SSCs constructed by FTO/bl-$TiO_2$ (blocking $TiO_2$)/mp-$TiO_2$/PbS CQDs/P3HT (poly-3-hexylthiophene)/PEDOT:PSS (poly(3,4-ethylenedioxythiophene) polystyrene sulfonate)/Au.[15] Seo *et al.* reported 3.2% mesoporous PbS QD/$CH_3NH_3PbI_3$ core/shell-SSCs.[16] Kim *et al.* reported 3.9% PbS QD-SSCs with radial

[a]*Functional Crystallization Center (ERC), Department of Chemical Engineering, Kyung Hee University, Yongin-si, Gyeonggi-do, Republic of Korea. E-mail: imromy@khu.ac.kr*
[b]*Department of Molecular Science and Technology, Ajou University, Suwon 443-749, Republic of Korea*
[c]*Department of Energy & Materials Engineering, Dongguk University, Seoul, Republic of Korea*

† Electronic supplementary information (ESI) available. See DOI: 10.1039/c6ra25637f

‡ These authors (J. H. Heo and M. H. Jang) have equally attributed to this work.

directional charge transport by using $TiO_2$ nanorod electron conductor instead of mp-$TiO_2$.[17] Very recently, Park *et al.* reported 8.07% mesoporous PbS embedding CuS QD-SSCs.[18]

On the other hand, the PbS QDs prepared by SILAR method did not have any insulating passivation layer on their surface due to direct grown on the mp-$TiO_2$. However, the SILAR method required tedious repeated process cycle: adsorption of cations (anions) → washing → drying → adsorption of anions (cations) → washing → drying. In addition, the size of PbS QDs deposited on mp-$TiO_2$ surface is not uniform because some tiny PbS nanoparticles are nucleated and grown on the mp-$TiO_2$ and at the same time the pre-deposited PbS nanoparticles are continuously overgrown by the repeated SILAR cycle, thereby deteriorating charge injection from PbS QDs into mp-$TiO_2$. To reduce the tedious repeated process cycle, Joo *et al.* devised a spin-assisted SILAR (spin-SILAR) method for fabricating a liquid-junction CdS-sensitized ZnO nanorod photoelectrochemical cell.[19] Im *et al.* reported the solid-state PbS-sensitized photovoltaic photodetectors and PbS–SSCs prepared by spin-SILAR.[20] By using spin-coating process instead of dipping process, the washing and drying process could be eliminated because the excess chemicals are automatically spun out and the film is dried during spin-coating process. However, it is still difficult to control the size uniformity of PbS QDs deposited on mp-$TiO_2$ *via* spin-SILAR. Therefore, here we tried to deposit more uniform PbS QDs on mp-$TiO_2$ *via* spin-assisted successive precipitation and anion exchange reaction (spin-SPAER) because the over growth of the pre-deposited PbS QDs on mp-$TiO_2$ can be reduced.

Fig. 1 is a schematic illustration of spin-SPARE process. For convention spin-SILAR, 5 mM $Pb(NO_3)_2/H_2O$/methanol ionic solution was used so that the $Pb^{2+}$ cations are adsorbed on mp-$TiO_2$ surface and then $Pb^{2+}$ cations are reacted with $S^{2-}$ anions to form PbS. During the repeated spin-SILAR process, the ions can be adsorbed on both mp-$TiO_2$ and pre-deposited PbS QDs. Accordingly, the size of PbS nanoparticles formed on mp-$TiO_2$ surface tends to be broadened as illustrated in upper right inset in Fig. 1 due to the formation of new PbS nuclei and the continuous overgrowth of pre-deposited PbS QDs. On the other hands, for spin-SPAER method 5 mM $PbX_2$ (X = I, Br, and Cl)/DMF solution instead of 5 mM $Pb(NO_3)_2/H_2O$/methanol ionic solution was spin-coated at 3000 rpm for 60 s. During the spin-coating process, the $PbX_2$ nanoparticles are precipitated on the surface of mp-$TiO_2$ (process I) as illustrated in Fig. 1. Then the $PbX_2$ is transformed into PbS by anion exchange reaction with 5 mM $Na_2S/H_2O$/methanol solution during second stage spin-coating process (process II) at 3000 rpm for 60 s. To prevent the deposition/precipitation of $PbX_2$ on pre-formed PbS on mp-$TiO_2$, 1 wt% 1,2 ethanedithiol (EDT)/ethanol solution was

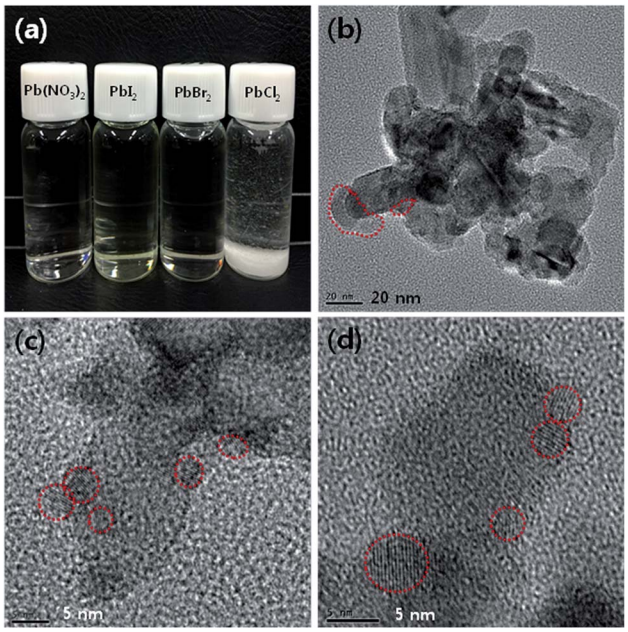


Fig. 2 (a) A photograph of 5 mM $Pb(NO_3)_2/H_2O$/methanol ionic solution and $PbX_2$ (X = I, Br, and Cl)/DMF solutions and (b–d) TEM (transmission electron microscopy) images of PbS nanoparticles deposited on mp-$TiO_2$, which are fabricated by 15 times repeated cycles of spin-SILAR process with 5 mM of $Pb(NO_3)_2/H_2O$/methanol ionic solution (b) and spin-SPAER process with 5 mM of $PbI_2$/DMF (c), and $PbBr_2$/DMF solution (d), respectively. Red dotted region = PbS nanoparticles.

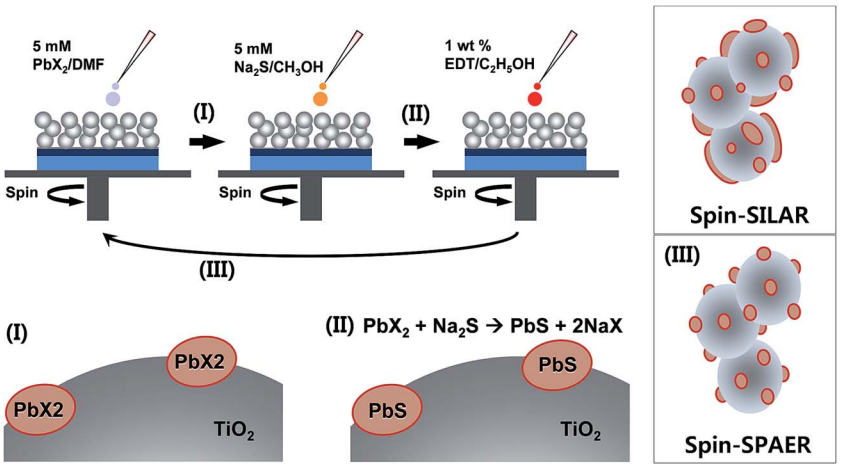


Fig. 1 Schematic illustration of spin-assisted successive precipitation and anion exchange reaction (spin-SPARE) process.

spin-coated at 3000 rpm for 60 s. By the repetition of the spin-SAER process (process III), we expect that the individual PbS QDs will be formed on mp-$TiO_2$ as illustrated in lower right inset in Fig. 1 because the $PbX_2$ precipitates cannot adsorbed on the pre-formed PbS QDs unlike to $Pb^{2+}$ cations.

Fig. 2(a) is a photograph of 5 mM $Pb(NO_3)_2/H_2O$/methanol ionic solution and $PbX_2$ (X = I, Br, and Cl)/DMF solutions showing that $Pb(NO_3)_2$, $PbI_2$, $PbBr_2$ are well dissolved in $H_2O$/methanol solution and DMF, respectively, whereas the 5 mM $PbCl_2$ is precipitated in DMF due to poor solubility. The order of solubility of $PbI_2$, $PbBr_2$, and $PbCl_2$ toward DMF solvent was $PbI_2$ > $PbBr_2$ > $PbCl_2$. Therefore, we excluded the $PbCl_2$/DMF solution for further model experiments. Fig. 2(b)–(d) are TEM (transmission electron microscopy) images of PbS nanoparticles deposited on mp-$TiO_2$, which are fabricated by 15 times repeated cycles of spin-SPAER process with 5 mM of $Pb(NO_3)_2/H_2O$/methanol ionic solution, $PbI_2$/DMF, and $PbBr_2$/DMF solution, respectively. The PbS nanoparticles deposited on mp-$TiO_2$ from 5 mM of $Pb(NO_3)_2/H_2O$/methanol ionic solution had polydispersed size (see Fig. 2(b)). Most PbS nanoparticles had below 5 nm but they are aggregated on mp-$TiO_2$ and some PbS nanoparticles had over 5 nm in size. Accordingly the energetic electron injection from PbS nanoparticles into mp-$TiO_2$ will be deteriorated by relatively large PbS nanoparticles because the conduction band edge of PbS nanoparticles with larger size become lower than the conduction band edge of mp-$TiO_2$.[21] On the other hands, the PbS QDs prepared from 5 mM $PbI_2$/DMF and $PbBr_2$/DMF solution showed smaller PbS nanoparticles with 3–5 nm in size (see Fig. 2(c and d)) and over grown PbS nanoparticles were not detected as shown in Fig. S1.† Apparently, the size PbS QDs deposited on mp-$TiO_2$ from $PbBr_2$/DMF solution seems to be slightly smaller than that from $PbI_2$/DMF solution, which might be attributed to the quicker precipitation (nucleation) of $PbBr_2$ than $PbI_2$ during spin-coating process. It should be noted that the individual PbS QDs without over growth are formed on mp-$TiO_2$ *via* spin-SPAER process as we proposed.

Fig. 3(a) is a representative SEM (scanning electron microscopy) cross-sectional image of PbS QD-SSC of which the PbS QDs are prepared by 15 times repeated cycles of spin-SPAER process with 5 mM of $PbBr_2$/DMF solution. The PbS QD-SSC was constructed by FTO/bl-$TiO_2$ (~50 nm in thickness)/mp-$TiO_2$ (~600 nm in thickness)/PbS QDs/P3HT (~30 nm in thickness)/Au (~60 nm in thickness). An energy band diagram of PbS QD-SSC was shown in Fig. 3(b). Upon illumination of light, the PbS QDs generate electron–hole pairs and the

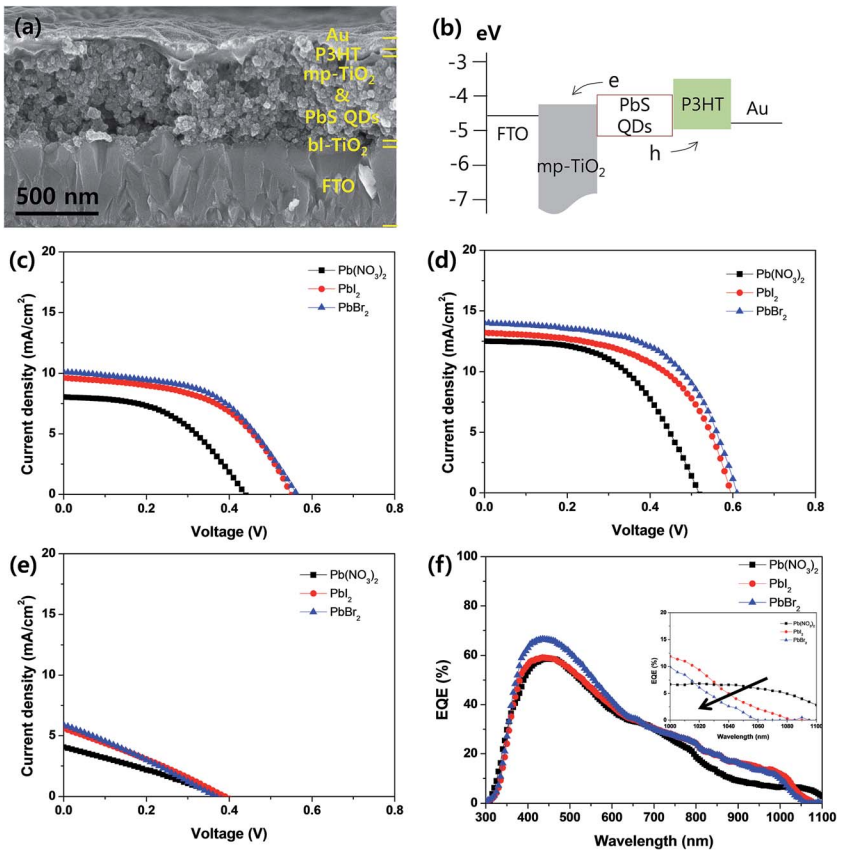


Fig. 3 (a) SEM (scanning electron microscopy) cross-sectional image of representative PbS QD-SSC composed to FTO/bl-$TiO_2$/mp-$TiO_2$/PbS QDs/P3HT/Au:PbS QDs are formed by 15 times repeated spin-SPAER process with 5 mM $PbBr_2$/DMF solution, (b) schematic energy band diagram, (c and d) current density–voltage (*J*–*V*) curves of PbS QD-SSCs with repeated coating cycles to (c) 10, (d) 15, and (e) 20 times of spin-SILAR ($Pb(NO_3)_2$) or spin-SPAER ($PbI_2$, $PbBr_2$) process, and (f) their corresponding EQE (external quantum efficiency) spectra: inset = zoom in at long wavelength region.

 

Table 1 Summary of photovoltaic properties of PbS QD-SSCs prepared by conventional spin-SILAR ($Pb(NO_3)_2$) and newly proposed spin-SPAER process ($PbI_2$ and $PbBr_2$)

| Repeated cycles | Device | $V_{oc}$ (V) | $J_{sc}$ (mA cm$^{-2}$) | FF (%) | $\eta$ (%) |
|---|---|---|---|---|---|
| 10 | $Pb(NO_3)_2$ | 0.43 | 8.0 | 50 | 1.72 |
| | $PbI_2$ | 0.54 | 9.6 | 53 | 2.75 |
| | $PbBr_2$ | 0.56 | 10.1 | 52 | 2.94 |
| 15 | $Pb(NO_3)_2$ | 0.51 | 12.5 | 54 | 3.44 |
| | $PbI_2$ | 0.59 | 13.2 | 56 | 4.36 |
| | $PbBr_2$ | 0.60 | 14.0 | 59 | 4.96 |
| 20 | $Pb(NO_3)_2$ | 0.38 | 4.1 | 29 | 0.45 |
| | $PbI_2$ | 0.39 | 5.6 | 28 | 0.61 |
| | $PbBr_2$ | 0.36 | 5.9 | 28 | 0.59 |

electrons (holes) are promptly transfer/transported into mp-$TiO_2$ (P3HT), respectively. If the size of PbS QDs is fluctuated, the conduction band edge of PbS QDs is fluctuated so that the driving force of electron injection from PbS QDs into mp-$TiO_2$ is dependent on the fluctuation. Fig. 3(c–e) compared the current density–voltage ($J$–$V$) curves of PbS QD-SSCs prepared by conventional spin-SILAR and newly proposed spin-SPAER process. Their photovoltaic properties were summarized in Table 1. To optimize efficiency of mode devices and check the tendency of the effect of spin-SPAER process, we fabricated PbS QD-SSCs with different repeated cycles for the formation of PbS QDs. For the model experiments, we controlled the repeated cycles of spin-SILAR and spin-SPAER to 10 (Fig. 3(c)), 15 (Fig. 3(d)), and 20 times (Fig. 3(e)), respectively. Irrespective to the repeated cycles for the formation of PbS QDs, the PbS QD-SSCs prepared by spin-SPAER process showed better device performance than that prepared by spin-SILAR process. The improved performance of PbS QD-SSCs prepared by spin-SPAER process is attributed to the formation of more uniform PbS-QDs on mp-$TiO_2$. Eventually the PbS QD-SSCs prepared by 15 times repeated cycles of spin-SILAR and spin-SPAER process exhibited the best device performance. The $Pb(NO_3)_2$ sample prepared by spin-SILAR process showed 0.51 V open-circuit voltage ($V_{oc}$), 12.5 mA cm$^{-2}$ short-circuit current density ($J_{sc}$), 54% fill factor (FF), and 3.44% power conversion efficiency ($\eta$). The $PbI_2$ and $PbBr_2$ samples prepared by spin-SPAER process showed 0.59 V $V_{oc}$, 13.2 mA cm$^{-2}$ $J_{sc}$, 56% FF, and 4.36% $\eta$ and 0.60 V $V_{oc}$, 14.0 mA cm$^{-2}$ $J_{sc}$, 59% FF, and 4.96% $\eta$ at 1 Sun condition, respectively. Therefore, the best $PbBr_2$ sample had improvement of 18% $V_{oc}$, 12% $J_{sc}$, 9% FF, and 44% $\eta$ compared to the $Pb(NO_3)_2$ device (see Table 1). The significant degradation of the performance in the PbS QD-SSCs with repeated coating cycles to 20 might be attributed to the formation of larger particles and the clogging of mesopores because the charge injection from large PbS sensitizer into mesoporous $TiO_2$ will be significantly deteriorated by the mismatch of energy band and the hole extraction efficiency will be also greatly deteriorated by the ineffective infiltration of P3HT hole transporting material with the mesopores in mesoporous $TiO_2$ film. Fig. 3(f) is EQE (external quantum efficiency) spectra of best devices (Fig. 3(d) samples). The calculated $J_{sc}$ values from the integration of the EQE spectra of $Pb(NO_3)_2$, $PbI_2$, and $PbBr_2$ sample was 12.1, 13.0, and 13.7 mA cm$^{-2}$, respectively so that these values were well matched to the measured $J_{sc}$ values in $J$–$V$ curves. The inset in Fig. 3(f) is the zoomed in EQE spectra around the band edge indicates that the onset wavelength of EQE spectrum is gradually blue-shifted in the order to $Pb(NO_3)_2$, $PbI_2$, and $PbBr_2$ sample. This implies that the average size of PbS QDs deposited on mp-$TiO_2$ is gradually decreased in the order to $Pb(NO_3)_2$, $PbI_2$, and $PbBr_2$ sample. This result is consistent with the TEM analysis in Fig. 2(b–d).

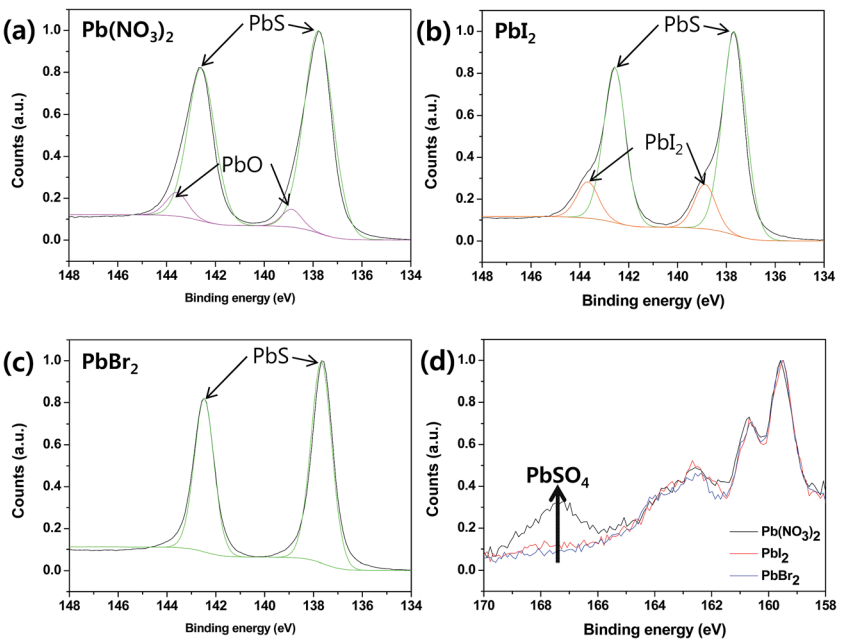


Fig. 4 XPS (X-ray photoelectron spectroscopy) spectra $Pb_{2p}$ (a–c) and $S_{2p}$ (d) peaks of PbS prepared by (a) $Pb(NO_3)_2$, (b) $PbI_2$, and (c) $PbBr_2$.

The electronic bandgap ($E_g$) of PbS QDs with a diameter ($d$) can be expressed by following equation.[22]

$$E_g = 0.41 + 1/(0.025d^2 + 0.283d)$$

From above equation, the calculated average diameter of $Pb(NO_3)_2$, $PbI_2$, and $PbBr_2$ sample was over 3.7 nm, ~3.6 nm, and ~3.5 nm, respectively. The EQE is a product of light harvesting efficiency ($\eta_{lhe}$), charge separation efficiency ($\eta_{cs}$), and charge collection efficiency ($\eta_{cc}$). The absorption spectra of $Pb(NO_3)_2$, $PbI_2$, and $PbBr_2$ sample did not have significant difference (see Fig. S2†). Accordingly, the EQE improvement by newly designed spin-SPAER process was mainly ascribed to the improved charge separation efficiency ($\eta_{cs}$) and charge collection efficiency ($\eta_{cc}$).

In addition, the PbS QD-SSCs prepared by spin-SPAER process was much better air stability than the PbS QD-SSC prepared by spin-SILAR process. Therefore, we checked the XPS (X-ray photoelectron spectroscopy) spectra of PbS QDs prepared by 15 times repeated cycles of spin-SILAR ($Pb(NO_3)_2$ sample) and spin-SPAER process ($PbI_2$ and $PbBr_2$ sample) after 1 week storage in air in order to check the purity and stability of PbS QDs as shown in Fig. 4. The PbS QDs prepared by spin-SILAR process ($Pb(NO_3)_2$ sample) exhibited PbO peak from the analysis of $Pb_{2p}$ peak analysis, whereas the PbS QDs prepared by spin-SPAER process ($PbI_2$ and $PbBr_2$ sample) did not show oxide peaks. In contrast, the PbS QDs prepared by spin-SPAER process using $PbI_2$ precursor exhibited $PbI_2$ peaks, whereas the PbS QDs prepared by using $PbBr_2$ precursor did not have $PbBr_2$ peaks. To distinguish the PbO peaks and $PbX_2$ (X = I, Br) peaks, we checked $X_{3d}$ peaks as shown in Fig. S3† because the binding energy of PbO and $PbX_2$ in $Pb_{2p}$ peaks is very close. Fig. S3† clearly confirms that the small quantity of $PbI_2$ was remained during spin-SPAER process, whereas the $PbBr_2$ impurity peaks were not detectable due to fully conversion into PbS QDs. The $S_{2p}$ peaks in Fig. 4(d) confirm that the PbS QDs prepared by spin-SILAR process were oxidized to PbO and $PbSO_4$, whereas the PbS QDs prepared by spin-SPAER were not oxidized. From these results, we can conclude that more efficient and stable PbS QD-SSCs could be fabricated by newly proposed spin-SPAER process.

## Conclusions

We could deposit relatively uniform PbS QDs *via* newly proposed spin-SPAER process whereas the conventional spin-SILAR process tends to form aggregated PbS QDs on mp-$TiO_2$ surface. The formation of individual PbS QDs on mp-$TiO_2$ by spin-SPAER might be attributed to the formation of nano-precipitates of $PbX_2$ (X = I, Br) so that the continuous over growth of PbS nanoparticles was suppressed. The solubility of $PbI_2$ in DMF solvent was higher than the $PbBr_2$ so that the size of nuclei of $PbI_2$ formed during spin-coating process will be bigger than the that of $PbBr_2$. Accordingly, the larger PbS QDs was formed by $PbI_2$ precursor than the $PbBr_2$. The EQE spectra of PbS QD-SSCs prepared by $Pb(NO_3)_2$, $PbI_2$, and $PbBr_2$ precursor indicated that the size of PbS QDs was gradually increased in the order to $PbBr_2 < PbI_2 < Pb(NO_3)_2$. Therefore, the overall power conversion efficiency of PbS QD-SSCs prepared by spin-SPAER process using $PbI_2$ and $PbBr_2$ precursor could be enhanced to ~26.7% and ~44.2%, respectively, compared to the PbS QD-SSCs prepared by spin-SILAR using $Pb(NO_3)_2$ precursor. From the XPS analysis, we could find that the PbS QD-SSCs prepared by spin-SPAER have better stability than the device prepared spin-SILAR because the surface of Pb or S in PbS QDs prepared by spin-SILAR is more easily oxidized into PbO or $PbSO_4$ whereas the PbS QDs prepared by spin-SPAER are not easily oxidized possibly due to the passivation by I or Br element.

## Acknowledgements

This study was supported by Basic Science Research Program (No. 2014R1A5A1009799), the Priority Research Program (2009-0093826) through the National Research Foundation of Korea (NRF) funded by the Ministry of Science, ICT & Future Planning and the New & Renewable Energy Core Technology Program (No. 20133030000140) of the Korea Institute of Energy Technology Evaluation and Planning (KETEP) granted financial resource from the Ministry of Trade, Industry & Energy.

## Notes and references

1 (*a*) H. J. Lee, M. K. Wang, P. Chen, D. R. Gamelin, S. M. Zakeeruddin, M. Grätzel and M. K. Nazeeruddin, *Nano Lett.*, 2009, **9**, 4221–4227; (*b*) L. Qu and X. Peng, *J. Am. Chem. Soc.*, 2002, **124**, 2049–2055; (*c*) I. Zarazúa, T. L. Luke, J. R. Gómez, A. T. Castro, J. Z. Zhang and E. D. l. Rosa, *J. Electrochem. Soc.*, 2014, **161**, H68–H74; (*d*) L. J. Diguna, Q. Shen, J. Kobayashi and T. Toyoda, *Appl. Phys. Lett.*, 2007, **91**, 23116; (*e*) C. B. Murray, D. J. Norris and M. G. Bawendi, *J. Am. Chem. Soc.*, 1993, **115**, 8706–8715; (*f*) C. M. Donegá, S. G. Hickey, S. F. Wuister, D. Vanmaekelbergh and A. Meijerink, *J. Phys. Chem. B*, 2003, **107**, 489–496.

2 (*a*) G. Y. Lan, Z. Yang, Y. W. Lin, Z. H. Lin, H. Y. Liao and H. T. Chang, *J. Mater. Chem.*, 2009, **19**, 2349–2355; (*b*) C. S. Ferekides, D. Marinskiy, V. Viswanathan, B. Tetali, V. Palekis, P. Selvaraj and D. L. Morel, *Thin Solid Films*, 2000, **361**, 520–526; (*c*) S. G. Kumar and K. S. R. K. Rao, *Energy Environ. Sci.*, 2014, **7**, 45–102; (*d*) J. Britt and C. Ferekides, *Appl. Phys. Lett.*, 1993, **62**, 2851–2852; (*e*) A. M. Hermann, *Sol. Energy Mater. Sol. Cells*, 1998, **55**, 75–81.

3 (*a*) R. J. Ellingson, M. C. Beard, J. C. Johnson, P. Yu, O. I. Micic, A. J. Nozik, A. Shabaev and A. L. Efros, *Nano Lett.*, 2005, **5**, 865–871; (*b*) F. D. Monte, Y. Xu and J. D. Mackenzie, *J. Sol-Gel Sci. Technol.*, 2000, **17**, 37–45; (*c*) Y. Pan, Y. R. Li, Y. Zhao and D. L. Akins, *J. Chem. Educ.*, 2015, **92**, 1860–1865; (*d*) H. Fu and S. W. Tsang, *Nanoscale*, 2012, **4**, 2187–2201; (*e*) E. J. D. Klem, H. Shukla, S. Hinds, D. D. Macneil, L. Levina and E. H. Sargent, *Appl. Phys. Lett.*, 2008, **92**, 212105.

 

4 (*a*) R. W. Crisp, D. M. Kroupa, A. R. Marshall, E. M. Miller, J. B. Zhang, M. C. Beard and J. M. Luther, *Sci. Rep.*, 2015, **5**, 9945; (*b*) J. B. Zhang, J. B. Gao, C. P. Church, E. M. Miller, J. M. Luther, V. I. Klimov and M. C. Beard, *Nano Lett.*, 2014, **14**, 6010–6015; (*c*) J. J. Choi, Y. F. Lim, M. B. S-Berrios, M. Oh, B. R. Hyun, L. F. Sun, A. C. Bartnik, A. Goedhart, G. G. Malliaras, H. D. Abruña, F. W. Wise and T. Hanrath, *Nano Lett.*, 2009, **9**, 3749–3755; (*d*) X. Zhang, Y. Zhang, L. Yan, C. Y. Ji, H. Wu, Y. Wang, T. Q. Zhang, Y. D. Wang, T. Cui, J. Zhao and W. W. Yu, *J. Mater. Chem. A*, 2015, **3**, 8501–8507; (*e*) M. Law, M. C. Beard, S. G. Choi, J. M. Luther, M. C. Hanna and A. J. Nozik, *Nano Lett.*, 2008, **8**, 3904–3910.

5 (*a*) D. H. Kim, S. J. Lee, M. S. Park, J. K. Kang, J. H. Heo, S. H. Im and S. J. Sung, *Nanoscale*, 2014, **6**, 14549–14554; (*b*) Y. C. Choi, D. U. Lee, J. H. Noh, E. K. Kim and S. I. Seok, *Adv. Mater.*, 2014, **24**, 3587–3592; (*c*) Y. Itzhaik, O. Niitsoo, M. Page and G. Hodes, *J. Phys. Chem. C*, 2009, **113**, 4254–4256; (*d*) S. Ito, K. Tsujimoto, D. C. Nguyen, K. Manabe and H. Nichino, *Int. J. Hydrogen Energy*, 2013, **38**, 16749–16754; (*e*) N. Dematage, E. V. A. Premalal and A. Konno, *Int. J. Electrochem. Sci.*, 2014, **9**, 1729–1737.

6 (*a*) Y. Zhou, L. Wang, S. Chen, S. Qin, X. S. Liu, J. Chen, D. J. Xue, M. Luo, Y. Cao, Y. Cheng, E. H. Sargent and J. Tang, *Nat. Photonics*, 2015, **9**, 409–415; (*b*) L. Efthimiopoulos, J. Zhang, M. Kucway, C. Y. Park, R. C. Ewing and Y. Wang, *Sci. Rep.*, 2013, **3**, 2665; (*c*) V. L. Deringer, R. P. Stoffel, M. Wuttig and R. Dronskowski, *Chem. Sci.*, 2015, **6**, 5255–5262; (*d*) F. A. E-Salam, M. Afifi and E. A. E-Wahabb, *Vacuum*, 1993, **44**, 111–116; (*e*) X. Liu, J. Chen, M. Luo, M. Leng, Z. Xia, Y. Zhou, S. Qin, D. J. Xue, L. Lv, H. Huang, D. Niu and J. Tang, *Appl. Mater. Interfaces*, 2014, **6**, 10687–10695.

7 (*a*) B. Yang, D. J. Xue, M. Leng, J. Zhong, L. Wang, H. Song, Y. Zhou and J. Tang, *Sci. Rep.*, 2015, **5**, 10978; (*b*) Z. Xia, J. Zhong, M. Leng, L. Hu, D. J. Xue, B. Yang, Y. Zhou, X. Liu, S. Qin, Y. B. Cheng and J. Tang, *Chem. Mater.*, 2015, **27**, 8048–8057.

8 (*a*) M. Chen, L. Shao, S. V. Kershaw, H. Yu, J. Wang, A. L. Rogach and N. Zhao, *ACS Nano*, 2014, **8**, 8208–8216; (*b*) S. Keuleyan, E. Lhuillier and P. G. Sionnest, *J. Am. Chem. Soc.*, 2011, **133**, 16422–16424; (*c*) S. Keuleyan, E. Lhuillier, V. Brajuskovic and P. G. Sionnest, *Nat. Photonics*, 2011, **5**, 489–493; (*d*) S. H. Im, H. J. Kin, S. W. Kim, S. W. Kim and S. I. Seok, *Nanoscale*, 2012, **4**, 1581–1584; (*e*) M. Chen, H. Yu, S. V. Kershaw, H. Xu, S. Gupta, F. Hetsch, A. L. Rogach and N. Zhao, *Adv. Mater.*, 2014, **24**, 1032–1037.

9 (*a*) T. J. Gillespie, C. H. Marshall, M. Contreras and J. Keane, *Sol. Energy Mater. Sol. Cells*, 1999, **59**, 27–34; (*b*) J. W. Yang, J. Y. Kim, J. H. Yu, T. Y. Ahn, H. J. Lee, T. S. Choi, Y. W. Kim, J. Joo, M. J. Ko and T. G. Hyeon, *Phys. Chem. Chem. Phys.*, 2013, **15**, 20517–20525; (*c*) K. J. Kim, R. P. Oleksak, C. Pan, M. W. Knapp, P. B. Kreider, G. S. Herman and C. H. Chang, *RSC Adv.*, 2014, **4**, 16418–16424; (*d*) B. M. Basol, V. K. Kapur, A. Halani and C. Leidholm, *Sol. Energy Mater. Sol. Cells*, 1993, **29**, 163–173.

10 S. W. Kim, M. J. Kang, S. J. Kim, J. H. Heo, J. H. Noh, S. H. Im, S. I. Seok and S. W. Kim, *ACS Nano*, 2013, **7**, 4756–4763.

11 (*a*) A. J. Nozik, M. C. Beard, J. M. Luther, M. Law, R. J. Ellingson and J. C. Johnson, *Chem. Rev.*, 2010, **110**, 6873–6890; (*b*) P. V. Kamat, *J. Phys. Chem. C*, 2008, **112**, 18737–18753; (*c*) B. Farrow and P. V. Kamat, *J. Am. Chem. Soc.*, 2009, **131**, 11124–11131; (*d*) W. A. Tisdale, K. J. Williams, B. A. Timp, D. J. Norris, E. S. Andil and X. Y. Zhu, *Science*, 2010, **328**, 1543–1547; (*e*) R. D. Schaller and V. I. Klimov, *Phys. Rev. Lett.*, 2004, **92**, 186601.

12 (*a*) C. Piliego, L. Protesescu, S. Z. Bisri, M. V. Kovalenko and M. A. Loi, *Energy Environ. Sci.*, 2013, **6**, 3054–3059; (*b*) N. Zhao, T. P. Osedach, L. Y. Chang, S. M. Geyer, D. Wanger, M. T. Binda, A. C. Arango, M. G. Bawendi and V. Bulovic, *ACS Nano*, 2010, **4**, 3743–3752; (*c*) A. S. Obaid, A. A. Dihe, B. M. Salih, Z. Hassan, Y. Aldourin and M. Bououdina, *Adv. Mater.*, 2014, **925**, 605–609.

13 (*a*) A. G. P. Abraham, I. J. Kramer, A. R. Barkhouse, X. Wang, G. Konstantatos, R. Debnath, L. Levina, I. Raabe, M. K. Nazeeruddin, M. Grätzel and E. H. Sargent, *ACS Nano*, 2010, **4**, 3374–3380; (*b*) M. Philip and N. Cowern, *International Renewable and Sustainable Energy Conference*, 2014, pp. 32–36; (*c*) J. Shi, P. Zhao and X. Wang, *Adv. Mater.*, 2013, **25**, 916–921; (*d*) M. M. Tavakoli, H. Aashuri, A. Simchi and Z. Fan, *Phys. Chem. Chem. Phys.*, 2015, **17**, 24412–24419; (*e*) B. A. Gonfa, H. Zhao, J. Li, J. Qiu, M. Saidani, S. Zhang, R. Izquierdo, N. Wu, M. A. E. Khakani and D. Ma, *Sol. Energy Mater. Sol. Cells*, 2014, **124**, 67–74.

14 (*a*) G. Niu, L. Wang, R. Gao, B. Ma, H. Dong and Y. Qiu, *J. Mater. Chem.*, 2012, **22**, 16914–16919; (*b*) S. D. Sung, L. S. Lim, P. Kang, C. M. Lee and W. I. Lee, *Chem. Commun.*, 2013, **49**, 6054–6056; (*c*) J. W. Lee, D. Y. Son, T. K. Ahn, H. W. Shin, I. Y. Kim, S. J. Hwang, M. J. Ko, S. H. Sul, H. S. Han and N. G. Park, *Sci. Rep.*, 2013, **3**, 1050.

15 S. H. Im, H. J. Kim, S. W. Kim, S. W. Kim and S. I. Seok, *Energy Environ. Sci.*, 2011, **4**, 4181–4186.

16 G. S. Seo, J. W. Seo, S. C. Ryu, W. P. Yin, T. K. Ahn and S. I. Seok, *J. Phys. Chem. Lett.*, 2014, **5**, 2015–2020.

17 S. W. Kim, J. H. Heo, J. H. Noh, S. W. Kim, S. H. Im and S. I. Seok, *ChemPhysChem*, 2014, **15**, 1024–1027.

18 J. P. Park, J. H. Heo, S. H. Im and S. W. Kim, *J. Mater. Chem. A*, 2015, **4**, 785–790.

19 J. Joo, D. Kim, D. J. Yun, H. Jun, S. W. Rhee, J. S. Lee, K. Yong, S. Kim and S. Jeon, *Nanotechnology*, 2010, **21**, 325604.

20 S. H. Im, H. J. Kim, S. W. Kim, S. W. Kim and S. I. Seok, *Org. Electron.*, 2012, **13**, 2352–2357.

21 S. H. Im, H. J. Kim and S. I. Seok, *Nanotechnology*, 2011, **22**, 395502.

22 B. R. Hyun, Y. W. Zhong, A. C. Bartnik, L. Sun, H. D. AbruÇa, F. W. Wise, J. D. Goodreau, J. R. Matthews, T. M. Leslie and N. F. Borrelli, *ACS Nano*, 2008, **2**, 2206–2212.